Scanning Electron Microscopy

Volume 1985
Number 2 *Part II*

Article 21

6-15-1985

Application of Chelex Standard Beads in Integrated Morphometrical and X-Ray Microanalysis

W. C. De Bruijn
Centre for Analytical Electron Microscopy, Leiden, The Netherlands

M. I. Cleton-Soeteman
Centre for Analytical Electron Microscopy, Leiden, The Netherlands

Follow this and additional works at: https://digitalcommons.usu.edu/electron

 Part of the Biology Commons

Recommended Citation

De Bruijn, W. C. and Cleton-Soeteman, M. I. (1985) "Application of Chelex Standard Beads in Integrated Morphometrical and X-Ray Microanalysis," *Scanning Electron Microscopy*: Vol. 1985 : No. 2 , Article 21.
Available at: https://digitalcommons.usu.edu/electron/vol1985/iss2/21

This Article is brought to you for free and open access by the Western Dairy Center at DigitalCommons@USU. It has been accepted for inclusion in Scanning Electron Microscopy by an authorized administrator of DigitalCommons@USU. For more information, please contact digitalcommons@usu.edu.

SCANNING ELECTRON MICROSCOPY/1985/II (Pages 715-729)
SEM Inc., AMF O'Hare (Chicago), IL 60666 USA

0586-5581/85$1.00+.05

APPLICATION OF CHELEX STANDARD BEADS IN INTEGRATED MORPHOMETRICAL AND X-RAY MICROANALYSIS

W.C. de Bruijn* and M.I. Cleton-Soeteman

Centre for Analytical Electron Microscopy,
Laboratory for Electron Microscopy,
Rijnsburgerweg 10, 2333 AA Leiden, The Netherlands

(Paper received February 13 1985, Completed manuscript received June 15 1985)

Abstract

Chelex ion exchange beads loaded with a known amount (18.3% weight percentage (w/w)) of platinum, have been co-embedded with a mouse peritoneal cell population. To establish the influence of the various deconvolution methods applied, upon the platinum concentration in cytoplasmic granules and erythrocytes these cross-sectioned beads are used as a standard. It is concluded that irrespective of the deconvolution method chosen 1) the Pt concentration inside the particles is identical when the particles and the co-embedded Chelex Pt standard, are analysed strictly under the same instrumental conditions 2) the Pt concentration outside the particle is zero, or virtually zero when that element is absent there (erythrocyte surrounded by Epon) 3) the Pt concentration outside the particle in the surrounding cytoplasm was identical (when the element Pt was present there).

The information about the elemental concentration obtained by point analysis in the STEM-mode in homogeneous objects was compared with the mean value obtained by the reduced raster method. The ratio between these values were constant.

As an example of a heteromorphic, heterogeneous cell organelle population, the application of the method of integrated morphometrical and chemical (X-ray) analysis is demonstrated on lysosomes within a single human liver parenchymal cell, containing iron and cerium. It was shown that the cerium concentration (from the cytochemical reaction to detect acid phosphatase activity in lysosomes) was rather homogeneously distributed over the small population and in the individual lysosomes. The iron distribution was very inhomogeneous, both in its distribution over the lysosomal area, and among the lysosomes in the population.

KEY WORDS: Chelex standards, electron microscopy, X-ray microanalysis, morphometry, image analysis, iron storage disease, peroxidase reaction, signal integration, H_2PtCl_6, diaminobenzidine

*Address for correspondence:
Centre for Analytical Electron Microscopy, Laboratory for Electron Microscopy, Rijnsburgerweg 10, 2333 AA Leiden, The Netherlands

Phone no. 31.71.148333 ext. 4666

Introduction

Recently, the method of integrated morphometrical and chemical analysis was proposed that enabled the simultaneous determination of both the area of cytoplasmic particles and the concentration of the elements present therein (4, 6, 7). The method was based upon the acquisition of net-intensity values within a small (reduced raster) area, containing the particle to be analysed, leading to elemental net-intensity distribution maps. The reliability of the chemical information "inside the particle" is determined by the method applied to separate the area in the X-ray spectrum containing the specific elemental counts from the concomitantly obtained continuum counts. Whereas the same action must also give realistic information about the same element "outside the particle", which might range from zero to almost the value "inside" the particle.

In the first paper (7) we had to prove, using an unconventional method, that such a separation could be performed, on line, during the acquisition of the reduced rastered area. The aim of the present study is to demonstrate that the net-intensity values obtained per pixelpoint, from this unconventional method, can be compared with the methods commonly available for quantification in off-line procedures. This will be demonstrated on Pt-containing erythrocytes and granules of eosinophilic granulocytes, in a mouse peritoneal cell population.

For the quantification of chemical elements we used Chelex ion exchange beads which, loaded with a known amount of the requested element(s), are present in the same ultrathin section (3,4,5). Although the use of the co-embedded Chelex standard is outlined before (6), this paper will illustrate that practical (deconvolution) problems can be alleviated by their application. However, it will be discussed that any other calibration system having the same type of abilities, can do the job equally well (2, 9). Secondly, the homogeneity of the platinum distribution over a Chelex Pt-standard bead, present in these ultrathin sections, will be tested. Thirdly, using homogeneous objects, the element concentration obtained by point analyses will be compared with the mean value acquired by the integrated method. Lastly, the

integrated method will be applied in the analysis of a population of iron containing lysosomes in a human liver parenchymal cell. The iron concentration in such lysosomes has been related to the cerium concentration of the acid phosphatase activity. Both elements are inhomogeneously distributed over the rather heteromorph organelles.

Materials and Methods

The analytical electron microscope (Philips EM 400) is equipped with a backscattered-electron ring detector, and a (STEM)-detector in combination with a Tracor Northern TN 2000 system. Stray apertures are present to reduce spurious X-rays, where possible. The ultrathin sections are mounted on Formvar-film covered 70 mesh copper grids in a beryllium low-background holder. In the specimen plate of the microscope, the side-entry goniometer and the X-ray detector are mounted on the same horizontal plane. The axis of the holder is situated perpendicular to the axis of the X-ray detector. The holder in the goniometer is tilted 18-24^{0} towards the energy dispersive SiLi-detector, mounted with 24^{0} tilt with respect to the horizontal plane.

For the performance of the digital-controlled raster analyses, a TN 1310-unit is added to the computer system. With this unit the electron beam can be directed over the specimen in a line or raster pattern by computer control. A colour screen assists in the visualization of the acquired images, the printer/plotter is used in the morphological integration process of the electron-image- and X-ray net-intensity arrays.

For the conventional X-ray analysis, the computer of the TN 2000 is loaded with the normal TN programs. The cellular material treated with the previously described tissue processing procedure (7) was used to solve the above-mentioned deconvolution problem. A new program called "reduced raster" mainly based upon the original IPP-ideas, was used as it has advantages for the integrated morphometrical analysis of heteromorphic, heterogeneous biological material, in combination with chemical analysis.

For the deconvolution of the continuum X-ray contribution under the peak area of the specific X-rays in the spectrum, four methods are available:

1. Energy filtering method (present in our Tracor Northern 2000); see (8).
2. Subtraction of a calculated complete "continuum-radiation" spectrum.
3. Subtraction of a calculated background region based upon two windows set in peak-free regions of the spectrum at either side of the peak region (DBL-method = double region subtraction method). This method is also described as the "linear"-method (1).
4. Subtraction of one single peak-free background region (SRS-method = single region subtraction method).

During the design of the integration program we chose the last option, to ensure that on-line performance was possible (7). Two versions were applied:

a) the peak-free background region to be subtracted was located at the very lowest end of the energy range of the spectrum (200-600 eV), leading to more or less "gross" intensity values (10)

b) a peak-free background region anywhere in the spectrum was selected such that after subtraction of that region from the requested peak region, the net-intensity value obtained matched the net-intensity value calculated by the energy filtering method (1) normally applied during quantitative deconvolution. It was clear that the a)-method underestimated the background under the peak, whereas the b)-method contained the risk to overestimate the background, especially at pixelpoints outside the particle. This was compensated by setting all negative values obtained after subtraction to zero (underflow-suppression). As the computer program has the ability to compare four regions of interest in the spectrum, background regions can be handled as if they were peak regions. So to be able to test the value of the DBL-method (3), two background regions at either side of the elemental peak were introduced and handled as pseudopeaks. The DBL-results were compared to those obtained by version b) of option 4) (SRS-method). As the program is designed to operate only when a background region (Bgr) is subtracted from any peak region, the virtually empty zero-region (200-600 eV) was offered to be subtracted "on line" from all regions. In the first experiment the position of one pseudopeak region (Bgr LI) was selected in such a way that, after its subtraction of the Pt(Lα) peak, the net-intensity content was approximately the same as that obtained by the energy-filter method and in that way could be used for the SRS-method. In the other experiments the SRS-method was applied to the Pt(Mα) peak, with a single background installed (Bgr*) to be subtracted according to the same criteria. When the arrays are acquired, the delineation of the particles from their surrounding is performed by the introduction of a figure (actually counts/pixelpoint/second). Two modes are operative to obtain the delineation of the particle: 1) selecting any figure from the original array. In this case the overlay image superimposed = original image (see Figs. 2 and 3, 7, and 8 and 11); 2) a delineation figure obtained and used in one of the other arrays is introduced, and the delineation from that array is superimposed (original image ≠ the overlay image; see Figs. 4 and 5; 9 and 10 or 13 and 14). In the pseudo-peak arrays (LI or RE), the true Pt-particle delineations from the PT or PM arrays are superimposed in that way. The selection of the figures to be introduced for the delineation are chosen prior to printing, guided by the image on the colour-screen.

Results

Comparison of the "SRS" and "DBL"-methods

In Fig. 1, the six regions used are indicated in a spectrum obtained from a 100 sec point analysis of an ultrathin sectioned erythrocyte, in which the peroxidatic activity is cytochemically converted into the presence of the element platinum. In addition to the platinum (Mα and Lα), the elements copper (from the grid-material) and silicon (assumed to be from the trough-water) are present. The peak and background regions used are hatched. The content of the four regions used

in experiment one are indicated in the top right hand corner. It includes six net-intensity values as calculated by the energy-filtering method, as performed by the TN 2000. In Figs. 2-5, four net-intensity arrays are shown from the same (16 x 16) erythrocyte-half acquired in one run (1 sec/point) by the reduced raster program. The Fig. 2-array is the Pt-Lα peak minus the background region (LI), indicated as PM (SRS-method). The Fig. 3-array is the Pt-Lα peak (minus the background region zero) indicated as PT. The Fig. 4-array is the background at the left side of the Pt-Lα-peak (LI), the Fig. 5-array the same at the right-hand side (RE) from the Pt-Lα minus the background zero region). In all four arrays delineations are present. In Fig. 2 the threshold value 15 c/p/s (counts/pixelpoint/sec) from the PM array is superimposed to separate the erythrocyte from the Pt-free surrounding Epon. In Figs. 3-5 the PT-threshold 15 c/p/s is shown.

For all arrays, the "inside" (IP) and "outside" (OP) particle mean ($\bar{X}$) plus the standard deviations are calculated. For the two true Pt-peaks involved (PT and PM), and the two pseudo-peak background regions (LI and RE), the "inside" mean net-intensity values were significantly different with respect to those calculated for the remaining "outside" points in the surrounding Epon (see top captions Figs. 2-5: P.value < 0.05).

From the Figs. 4 and 5-arrays (LI and RE) the true background under the Pt-Lα peak (Fig. 3 array) was reconstructed (by hand, off-line). The calculation applied to determine the background portion of the (Pt) Lα peak is outlined in Fig. 6. In short it is comprised of:

$$\bar{X}^{RE}_{Bgr.} + \frac{760}{3000} \cdot (\bar{X}^{LI}_{Bgr.} - \bar{X}^{RE}_{Bgr.}) = \bar{X}^{Pt\text{-}L\alpha}_{Bgr.} \text{ calculated} \quad (1)$$

From the mean "inside" values obtained, the mean true background under the Pt-Lα-peak was reconstructed, using this formula. The obtained calculated mean value (in c/p/s) was subtracted from the mean Pt-Lα-(gross) value (= peak plus background of the Pt-Lα-region minus the background region zero). This mean value is calculated from the array in Fig. 3. $\bar{X}$(Pt-Lα minus background region zero) minus $\bar{X}$ (background calculated under the Pt-Lα-peak) = Pt-Lα-net-intensity value. Similarly, using the "outside" mean values, the mean Pt-Lα net-intensity value of the areas outside the erythrocyte was calculated.
In Table 1 it can be seen that other thresholds values were also applied and in all cases the mean net Pt-Lα value according to the DBL-method was calculated for both the "inside" and "outside" values then obtained. In Figs. 2 and 3 the points included in the "innerpart" of the erythrocyte are indicated for the two thresholds applied (11 ←; 10 ↖). All mean net-intensity values (in c/p/s) were converted into c/p/s/nm^2 by dividing the values by the spot area (in nm^2). The inside values obtained by the DBL and the SRS method were not significantly different, and the "outside" values were low or virtually zero (Table 1 and Table 4). In a similar way, part of a cross section of a Chelex Pt-containing co-embedded bead was analyzed. But in this case the SRS-method was applied to the Pt-Mα region, with the special background region (Bgr*) to be subtracted and

Figures 2-5 are on the next page.

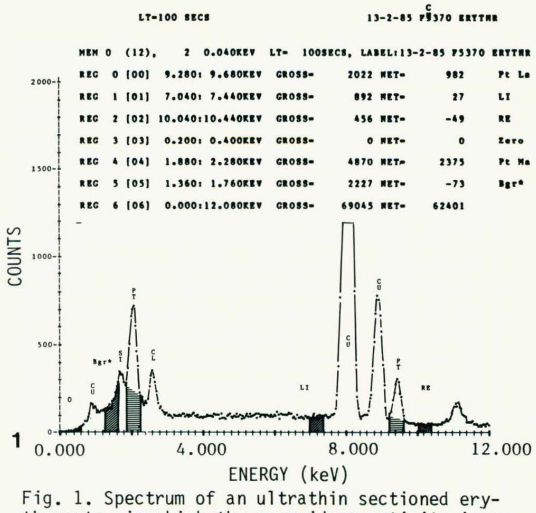

Fig. 1. Spectrum of an ultrathin sectioned erythrocyte, in which the peroxidase activity is converted into a platinum precipitate. In the (100 sec) point analysis-spectrum, the regions of interest used throughout the experiments described are indicated. Around the Pt-Lα peak region the background regions LI and RE are indicated. To the left of the Pt-Mα region the special background region Bgr*, used in experiments 2 and 3 for the SRS-method is present. The Zero region at the far left is subtracted from all regions during the on-line procedure. The content of the regions is given in the top of the spectrum (Filter method see 8).

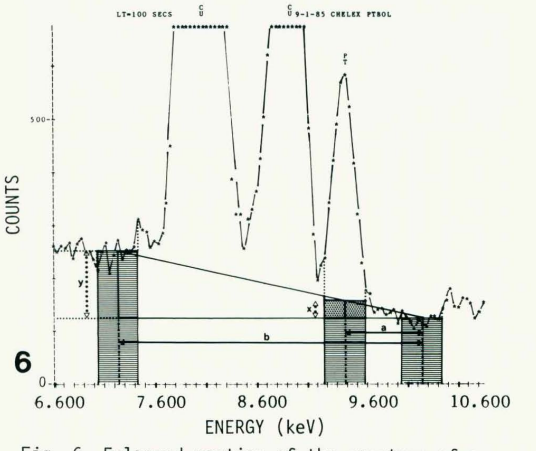

Fig. 6. Enlarged portion of the spectrum of a 100 sec point analysis of a Pt-containing Chelex-bead cross section containing the background regions LI and RE and the Pt-Lα-region, each 400 eV wide. The calculation of the background under the Pt-Lα-peak for the DBL-method is based upon the trigonal relation a/b = x/y (X = a.y/b). In which y = the mean value of background LI minus RE, and a and b are determined by the position of the mid-values of the regions in the spectrum.

ORIGINAL IMAGE:XRAY PM
OVERLAY IMAGE:XRAY PM OVERLAY THRESHOLD: 15
MAGNIFICATION: 37236 TOTAL AREA: 11269223 NM^2
LABEL:27-12-84 ERYTHROCYT 2 PT\BGR,LI\BGR RE\PT-BGR,LI

NUMBER OF POINTS(I P):130 | NUMBER OF POINTS(O P):126
MEAN (I P): 46.38 C/P | MEAN (O P): 1.97 C/P
S. DEVIATION (I P): 23.28 C/P | S. DEVIATION (O P): 2.47 C/P
MEAN+2S.D.(I P): 92.95 C/P | MEAN+2S.D.(O P): 6.93 C/P
DEGREES OF FREEDOM: 254 T-VALUE: 44.40 P ≤ 0.05
DWELL-TIME/POINT: 1000000 USEC.
SPOTAREA: 1963 NM^2 ANALYZED AREA 4.46 %
INTER PIXEL DISTANCE: 209 NM AREA(I P): 5722652 NM^2
[XRAY PM]= 2.36E-02 C/P/S/NM^2
[S. DEVIATION]= 1.18E-02 C/P/S/NM^2 C.V.= 50.20 %

SRS

2	0	2	44	59	51	50	49	55	48	67	41	51	17	10	0
2	0	2	52	74	44	42	32	31	56	34	31	43	27	14	0
2	0	2	32	46	53	43	29	42	24	63	43	42	42	15	0
11	0	2	44	43	66	46	31	39	52	42	32	79	65	11	0
2	0	2	42	58	51	47	32	39	45	58	28	55	66	22	3
7	0	2	39	71	77	55	36	50	44	38	44	59	72	22	7
2	0	2	35	50	23	46	38	39	59	58	63	66	69	22	6
2	0	2	19	43	55	43	48	51	27	47	60	46	60	3	0
2	0	2	11	30	40	59	52	42	48	58	64	79	27	2	1
2	2	2	0	27	36	51	41	39	61	63	55	42	3	2	0
2	0	2	0	6	34	30	44	47	41	51	46	23	0	2	0
2	0	2	4	2	17	38	51	50	34	38	18	7	0	2	0
2	0	3	1	2	0	3	19	27	25	2	0	2	1	2	0
2	0	2	0	2	0	2	0	2	0	2	0	2	0	3	5
3	2	2	0	2	0	2	3	2	2	2	2	6	0	2	0
2	2	0	2	1	2	0	2	0	2	0	2	4	2	0	2	3

Fig. 2. Reduced raster array from an erythrocyte half. The Pt-Lα array, (minus background LI). Threshold 15 has been superimposed. Other threshold figures are indicated. (11=◄;10=⇦). SRS-method.

ORIGINAL IMAGE:XRAY PT
OVERLAY IMAGE:XRAY PT OVERLAY THRESHOLD: 15
MAGNIFICATION: 37236 TOTAL AREA: 11269223 NM^2
LABEL:27-12-84 ERYTHROCYT 2 PT\BGR,LI\BGR RE\PT-BGR,LI

NUMBER OF POINTS(I P):135 NUMBER OF POINTS(O P):121
MEAN (I P): 56.16 C/P MEAN (O P): 4.58 C/P
S. DEVIATION (I P): 16.58 C/P S. DEVIATION (O P): 3.10 C/P
MEAN+2S.D.(I P): 89.32 C/P MEAN+2S.D.(O P): 10.78 C/P
DEGREES OF FREEDOM: 254 T-VALUE: 51.57 P ≤ 0.05
DWELL-TIME/POINT: 1000000 USEC.
SPOTAREA: 1963 NM^2 ANALYZED AREA 4.46 %
INTER PIXEL DISTANCE: 209 NM AREA(I P): 5942754 NM^2
[XRAY PT]= 2.86E-02 C/P/S/NM^2
[S. DEVIATION]= 8.44E-03 C/P/S/NM^2 C.V.= 29.52 %

DBL

2	3	5	59	74	73	60	62	71	57	70	61	65	31	17	0
5	2	8	62	85	67	53	41	46	68	48	58	66	48	23	1
6	6	5	49	62	66	59	40	58	50	75	57	58	50	22	2
10	6	7	62	63	81	55	45	47	69	54	48	94	77	22	0
10	6	7	58	78	65	63	41	50	51	71	45	58	80	30	1
15	3	7	51	87	89	71	46	63	60	54	59	71	81	35	2
3	7	6	46	59	42	59	52	47	71	62	79	79	82	22	4
11	1	6	35	58	75	58	58	67	47	59	71	63	69	10	1
2	0	7	18	38	57	66	63	55	65	79	78	91	35	6	3
2	11	6	0	42	50	63	57	55	72	74	64	54	13	3	1
3	4	6	4	15	41	47	59	54	53	62	55	35	1	6	0
3	3	3	9	6	35	54	65	54	50	47	27	6	3	2	0
2	5	10	7	6	4	14	29	34	30	10	0	2	7	7	1
3	0	3	2	2	6	3	9	3	3	3	1	2	5	7	2
7	7	3	2	2	6	6	6	6	6	7	5	11	2	6	3
3	2	0	7	7	3	4	3	2	10	2	6	6	10	6	6	1

Fig. 3. Reduced raster array of the same erythrocyte half. Pt-Lα-array (minus background Zero). Threshold 15 is superimposed, other threshold figures are indicated (11=◄;10=⇦). Used for DBL-method.

ORIGINAL IMAGE:XRAY LI
OVERLAY IMAGE:XRAY PT OVERLAY THRESHOLD: 15
MAGNIFICATION: 37236 TOTAL AREA: 11269223 NM^2
LABEL:27-12-84 ERYTHROCYT 2 PT\BGR,LI\BGR RE\PT-BGR,LI

NUMBER OF POINTS(I P):136 | NUMBER OF POINTS(O P):120
MEAN (I P): 13.55 C/P | MEAN (O P): 7.53 C/P
S. DEVIATION (I P): 4.57 C/P | S. DEVIATION (O P): 3.59 C/P
MEAN+2S.D.(I P): 22.71 C/P | MEAN+2S.D.(O P): 14.72 C/P
DEGREES OF FREEDOM: 254 T-VALUE: 6.02 P ≤ 0.05
DWELL-TIME/POINT: 1000000 USEC.
SPOTAREA: 1963 NM^2 ANALYZED AREA 4.46 %
INTER PIXEL DISTANCE: 209 NM AREA(I P): 5986774 NM^2
[XRAY LI]= 6.90E-03 C/P/S/NM^2
[S. DEVIATION]= 2.33E-03 C/P/S/NM^2 C.V.= 33.75 %

10	7	7	15	19	22	14	13	18	9	3	20	18	14	7	1
18	7	10	10	11	23	15	9	15	12	14	27	27	21	11	5
10	8	10	17	18	13	18	11	14	26	14	14	18	8	7	3
3	6	10	18	18	15	11	14	10	17	10	16	15	12	15	5
19	12	7	16	22	14	14	9	11	6	15	17	7	14	10	0
10	8	7	12	18	12	14	10	11	16	18	15	10	9	15	1
7	8	11	11	11	19	15	14	10	12	6	16	15	13	2	1
10	7	10	16	15	20	15	10	18	20	14	11	19	9	7	1
6	10	15	7	10	17	11	11	15	17	23	14	14	8	14	4
10	9	11	7	15	14	14	16	18	11	11	9	14	10	10	5
6	5	10	10	7	7	19	15	11	12	15	9	10	8	11	4
3	6	10	5	6	18	14	14	6	16	7	9	3	8	6	2
14	10	7	6	14	5	11	10	11	5	14	2	7	6	7	3
6	7	10	8	7	8	7	10	6	16	10	6	6	5	6	5
6	5	7	7	11	8	11	3	11	4	15	3	7	5	6	4
4	7	4	11	6	6	7	11	6	11	4	10	2	10	11	10	4

Fig. 4. Reduced raster array from the same erythrocyte half. Background LI-array (minus background Zero), with threshold 15 superimposed. Used for DBL-calculations, as outlined in Fig. 6.

ORIGINAL IMAGE:XRAY RE
OVERLAY IMAGE:XRAY PT OVERLAY THRESHOLD: 15
MAGNIFICATION: 37236 TOTAL AREA: 11269223 NM^2
LABEL:27-12-84 ERYTHROCYT 2 PT\BGR,LI\BGR RE\PT-BGR,LI

NUMBER OF POINTS(I P):134 | NUMBER OF POINTS(O P):122
MEAN (I P): 8.57 C/P | MEAN (O P): 4.52 C/P
S. DEVIATION (I P): 3.60 C/P | S. DEVIATION (O P): 2.61 C/P
MEAN+2S.D.(I P): 15.78 C/P | MEAN+2S.D.(O P): 9.75 C/P
DEGREES OF FREEDOM: 254 T-VALUE: 4.05 P ≤ 0.05
DWELL-TIME/POINT: 1000000 USEC.
SPOTAREA: 1963 NM^2 ANALYZED AREA 4.46 %
INTER PIXEL DISTANCE: 209 NM AREA(I P): 5898734 NM^2
[XRAY RE]= 4.36E-03 C/P/S/NM^2
[S. DEVIATION]= 1.83E-03 C/P/S/NM^2 C.V.= 42.07 %

3	5	7	12	6	10	19	8	14	7	15	3	10	10	3	3
10	7	6	3	7	13	6	3	6	7	10	8	11	7	7	1
3	5	7	8	10	10	15	7	10	7	10	12	7	0	6	2
6	6	6	11	15	11	14	9	6	17	6	15	10	7	7	3
6	5	3	9	10	12	10	12	7	6	3	7	7	13	10	0
2	6	3	5	6	4	10	9	10	10	15	7	10	14	11	3
6	0	10	3	11	6	15	13	6	11	7	11	11	7	2	1
3	1	10	9	7	8	6	7	11	13	3	7	19	4	7	4
2	3	3	2	10	15	14	6	6	8	10	10	10	6	6	3
3	5	7	0	6	7	14	7	10	10	7	5	7	5	6	4
7	5	7	6	6	5	10	8	7	12	6	10	3	9	11	3
2	5	3	6	2	6	10	10	2	7	6	6	2	3	2	0
2	7	6	5	3	6	7	4	2	8	7	6	6	4	7	3
2	0	2	4	2	2	6	4	2	12	3	4	6	2	7	5
6	3	3	3	6	7	2	1	10	2	3	5	7	1	3	3
5	2	2	10	8	6	9	3	3	6	9	7	4	6	2	6	4

Fig. 5. Reduced raster array from the same erythrocyte half. Background region RE (minus background region Zero), with threshold 15 superimposed. Used for DBL-calculation (see Fig. 6)

ORIGINAL IMAGE:XRAY PM
OVERLAY IMAGE:XRAY PM OVERLAY THRESHOLD: 15
MAGNIFICATION: 37236 TOTAL AREA: 11269223 NM^2
LABEL:CHELEX PT* 1-2-1985 HOEK EPON\VLIES

NUMBER OF POINTS(I P):207 | NUMBER OF POINTS(O P): 49
MEAN (I P): 59.40 C/P | MEAN (O P): 2.26 C/P
S. DEVIATION (I P): 26.41 C/P | S. DEVIATION (O P): 3.49 C/P
MEAN+2S.D.(I P): 112.24 C/P | MEAN+2S.D.(O P): 9.26 C/P
DEGREES OF FREEDOM: 254 | T-VALUE: 57.14 P ≤ 0.05
DWELL-TIME/POINT: 1000000 USEC.
SPOTAREA: 1963 NM^2 ANALYZED AREA 4.46 %
INTER PIXEL DISTANCE: 209 NM AREA(I P): 9112223 NM^2
[XRAY PM]= 3.02E-02 C/P/S/NM^2
[S. DEVIATION]= 1.34E-02 C/P/S/NM^2 C.V.= 44.46 %

SRS

	2	0	2	0	2	0	2	0	2	0	2	0	15	5	2	0
	2	10	15	0	2	0	2	0	2	12	2	29	38	5	2	0
	34	32	6	42	15	0	2	13	31	6	59	78	63	46	2	0
	55	45	31	66	59	43	58	30	39	22	50	29	62	27	11	0
	74	94	90	82	82	69	74	109	98	118	106	89	118	82	18	0
	99	110	83	78	102	78	94	88	75	122	90	97	98	60	47	1
	95	79	79	74	58	56	38	101	62	77	90	63	110	77	43	0
	62	69	87	76	54	75	95	82	71	70	54	77	79	67	50	0
	47	53	71	115	63	56	54	57	75	92	62	76	67	40	26	0
	31	40	75	52	50	60	63	47	67	59	51	56	66	63	31	5
	75	61	55	45	71	67	55	54	50	50	79	51	66	44	54	0
	22	46	38	65	43	70	66	68	75	50	58	59	59	36	43	0
	62	42	59	49	71	46	50	43	50	61	71	42	43	63	18	1
	39	34	59	23	38	46	30	55	82	65	22	27	30	52	11	0
	47	52	35	39	19	43	43	60	54	52	51	41	50	38	18	0
7	75	47	38	56	46	61	51	33	51	32	54	62	38	19	18	0

Fig. 7. Reduced raster array from a cross-sectioned Chelex standard. Pt-Mα array (minus background *), with threshold 15 superimposed. Other threshold figures are indicated (11=). SRS method.

ORIGINAL IMAGE:XRAY PT
OVERLAY IMAGE:XRAY PT OVERLAY THRESHOLD: 15
MAGNIFICATION: 37236 TOTAL AREA: 11269223 NM^2
LABEL:CHELEX PT* 1-2-1985 HOEK EPON\VLIES

NUMBER OF POINTS(I P):217 | NUMBER OF POINTS(O P): 39
MEAN (I P): 41.29 C/P | MEAN (O P): 6.48 C/P
S. DEVIATION (I P): 12.97 C/P | S. DEVIATION (O P): 4.51 C/P
MEAN+2S.D.(I P): 67.24 C/P | MEAN+2S.D.(O P): 15.51 C/P
DEGREES OF FREEDOM: 254 | T-VALUE: 34.80 P ≤ 0.05
DWELL-TIME/POINT: 1000000 USEC.
SPOTAREA: 1963 NM^2 ANALYZED AREA 4.46 %
INTER PIXEL DISTANCE: 209 NM AREA(I P): 9552427 NM^2
[XRAY PT]= 2.10E-02 C/P/S/NM^2
[S. DEVIATION]= 6.60E-03 C/P/S/NM^2 C.V.= 31.41 %

DBL

	9	7	12	8	10	7	16	16	11	7	11	4	16	13	7	3
	11	12	17	16	12	12	10	18	23	12	16	8	23	11	12	1
	23	24	21	19	24	27	22	27	30	20	18	15	26	16	10	0
	38	40	42	33	35	45	31	35	30	28	30	31	38	23	10	3
	74	64	55	74	54	47	58	63	71	53	63	53	70	52	18	0
	46	60	59	54	58	62	63	77	63	56	63	62	70	50	26	1
	55	46	46	52	47	60	79	45	51	47	46	55	47	42	38	4
	59	49	54	39	58	43	39	49	51	51	43	45	50	63	26	2
	54	37	35	42	42	40	51	36	54	48	46	44	51	59	46	2
	47	47	47	43	38	43	35	53	51	32	54	47	35	58	30	0
	47	44	35	40	54	38	50	44	39	40	51	30	43	33	31	4
	43	45	51	29	42	30	38	50	51	40	46	32	43	42	31	0
	39	45	34	34	39	30	43	35	46	35	38	33	31	38	26	0
	30	38	34	47	42	37	35	35	30	53	26	51	50	30	30	2
	42	37	35	40	34	35	47	22	42	38	31	42	43	39	31	3
8	38	35	34	23	51	35	38	45	31	36	39	33	38	45	26	2

Fig. 8. Reduced raster array from the same Chelex standard. Pt-Lα array(minus background Zero). Threshold 15 superimposed, with other threshold figures indicated (11=). Use for DBL-method.

ORIGINAL IMAGE:XRAY LI
OVERLAY IMAGE:XRAY PT OVERLAY THRESHOLD: 15
MAGNIFICATION: 37236 TOTAL AREA: 11269223 NM^2
LABEL:CHELEX PT* 1-2-1985 HOEK EPON\VLIES

NUMBER OF POINTS(I P):217 | NUMBER OF POINTS(O P): 39
MEAN (I P): 16.34 C/P | MEAN (O P): 8.94 C/P
S. DEVIATION (I P): 4.22 C/P | S. DEVIATION (O P): 4.88 C/P
MEAN+2S.D.(I P): 24.79 C/P | MEAN+2S.D.(O P): 18.71 C/P
DEGREES OF FREEDOM: 254 | T-VALUE: 7.39 P ≤ 0.05
DWELL-TIME/POINT: 1000000 USEC.
SPOTAREA: 1963 NM^2 ANALYZED AREA 4.46 %
INTER PIXEL DISTANCE: 209 NM AREA(I P): 9552427 NM^2
[XRAY LI]= 8.32E-03 C/P/S/NM^2
[S. DEVIATION]= 2.15E-03 C/P/S/NM^2 C.V.= 25.85 %

	11	11	14	11	18	23	10	11	15	11	10	10	18	10	6	8
	11	16	11	9	15	13	11	20	15	9	11	11	30	8	10	8
	19	11	22	13	14	21	18	21	11	12	15	13	18	14	14	1
	19	10	14	14	18	17	22	16	7	15	14	15	14	14	6	3
	18	19	18	19	22	12	18	18	22	14	14	16	10	19	11	4
	14	15	23	28	15	15	19	12	26	14	14	31	14	12	7	1
	19	16	14	23	11	24	15	24	22	17	18	17	22	22	10	7
	23	12	18	24	26	22	19	10	14	12	15	17	19	12	14	4
	19	17	19	20	22	17	14	17	15	20	19	21	19	16	15	3
	15	17	22	17	15	20	11	19	18	22	14	15	18	9	18	9
	18	18	15	15	11	8	19	21	19	16	14	15	18	15	10	6
	10	15	14	10	19	13	22	14	18	20	15	14	18	20	15	6
	14	18	15	12	18	17	18	19	10	20	18	15	14	20	11	6
	11	21	11	18	14	16	14	15	18	19	26	18	22	18	22	3
	19	16	11	16	14	19	15	15	18	22	19	15	14	16	10	3
9	19	9	14	13	15	23	18	10	14	16	10	10	15	11	14	3

Fig. 9. Reduced raster array from the same Chelex standard. Background LI (minus background Zero). Threshold 15 superimposed. Used for DBL calculation as outlined in Fig. 6.

ORIGINAL IMAGE:XRAY RE
OVERLAY IMAGE:XRAY PT OVERLAY THRESHOLD: 15
MAGNIFICATION: 37236 TOTAL AREA: 11269223 NM^2
LABEL:CHELEX PT* 1-2-1985 HOEK EPON\VLIES

NUMBER OF POINTS(I P):217 | NUMBER OF POINTS(O P): 39
MEAN (I P): 10.07 C/P | MEAN (O P): 6.02 C/P
S. DEVIATION (I P): 3.68 C/P | S. DEVIATION (O P): 2.82 C/P
MEAN+2S.D.(I P): 17.45 C/P | MEAN+2S.D.(O P): 11.67 C/P
DEGREES OF FREEDOM: 254 | T-VALUE: 4.04 P ≤ 0.05
DWELL-TIME/POINT: 1000000 USEC.
SPOTAREA: 1963 NM^2 ANALYZED AREA 4.46 %
INTER PIXEL DISTANCE: 209 NM AREA(I P): 9552427 NM^2
[XRAY RE]= 5.13E-03 C/P/S/NM^2
[S. DEVIATION]= 1.87E-03 C/P/S/NM^2 C.V.= 36.62 %

	7	7	10	6	6	11	6	13	7	10	15	8	10	4	7	5
	2	8	10	10	7	8	7	18	10	7	10	8	10	8	6	8
	7	7	6	6	11	7	14	11	3	12	7	10	11	3	7	4
	10	9	6	5	6	18	6	15	10	6	14	12	10	8	7	1
	7	8	10	15	18	10	19	11	11	10	11	8	19	9	2	4
	6	4	11	16	7	15	11	5	15	8	11	9	14	7	14	3
	10	14	7	11	15	12	11	10	22	8	15	14	10	18	3	6
	11	14	7	8	14	11	10	13	15	9	11	9	14	7	3	4
	6	10	11	21	11	9	11	13	7	5	11	14	14	11	11	4
	14	12	11	3	11	14	11	10	10	13	2	4	6	4	10	4
	14	9	19	7	7	9	10	13	10	13	6	3	10	9	11	5
	14	9	6	9	14	12	14	11	7	11	10	13	15	13	6	3
	7	8	10	8	11	5	14	2	11	9	14	8	6	7	7	3
	7	6	6	8	14	4	10	11	11	17	10	17	7	14	11	3
	10	8	11	9	15	11	14	8	6	6	11	7	7	10	7	4
10	11	10	11	8	11	10	6	12	10	9	11	11	14	7	7	1

Fig. 10. Reduced raster array from the same Chelex standard. Background RE (minus background Zero). Threshold 15 superimposed. Used for DBL calculation as outlined in Fig. 6.

TABLE 1
REDUCED RASTER ANALYSIS OF AN ERYTHROCYTE
AT 16 X 16 PIXELPOINTS

▼Original Image	▼Overlay Image	▼Threshold		INNER POINTS SRS-METHOD Mean Values c/p/s	INNER POINTS SRS-METHOD Unit Values c/p/s $nm^2 x10^{-3}$	OUTER POINTS Mean Values c/p/s	OUTER POINTS Unit Values c/p/s $nm^2/x10^{-3}$	AREA μm^2
PM	PM	15	$\bar{X}$	46.38	23.6	2.0	1.0	5.72
			SD	23.28	11.8	2.5	1.3	
,,	,,	11	$\bar{X}$	45.35	23.0	1.7	0.9	5.90
			SD	23.68	12.0	1.7	0.9	
,,	,,	10	X	45.08	22.9	1.6	0.8	5.94
			SD	23.79	12.1	1.6	0.8	
				DBL-METHOD				
PT	PT	15	$\bar{X}$	56.16	28.6	4.6	2.3	5.99
			SD	16.58	8.4	3.1	1.8	
LI	PT	15	$\bar{X}$	13.55	6.9	7.6	3.8	
			SD	4.57	2.3	3.6	1.8	
RE	PT	15	$\bar{X}$	8.57	4.4	4.5	2.3	
			SD	3.60	1.8	2.6	1.3	
	PT	15	$\bar{X}$-Calcul.		23.6		-0.4	
PT	PT	11	$\bar{X}$	58.24	29.6	4.3	2.2	6.16
			SD	28.53	14.5	2.7	1.4	
LI	PT	11	$\bar{X}$	13.44	6.9	7.5	3.8	
			SD	3.56	2.4	3.6	1.8	
RE	PT	11	$\bar{X}$	8.46	4.3	4.5	2.3	
			SD	3.60	1.8	2.6	1.3	
	PT	11	$\bar{X}$-Calcul.		24.7		-0.4	
PT	PM	15	$\bar{X}$	60.44	30.7	5.3	2.7	5.72
			SD	24.43	12.4	4.3	2.2	
LI	PM	15	$\bar{X}$	13.72	7.0	7.7	3.9	
			SD	4.58	2.3	2.6	1.8	
RE	PM	15	$\bar{X}$	8.73	4.4	4.5	2.3	
			SD	3.5	1.8	2.6	1.3	
	PM	15	$\bar{X}$-Calcul.		25.7		0.0	
PT	PM	11	$\bar{X}$	60.14	30.6	4.8	2.5	5.90
			SD	27.69	14.1	3.5	1.8	
LI	PM	11	$\bar{X}$	13.58	6.9	7.6	3.9	
			SD	4.65	2.4	3.5	1.8	
RE	PM	11	$\bar{X}$	8.63	4.4	4.5	2.3	
			SD	3.55	1.8	2.6	1.3	
		11	$\bar{X}$-Calcul.		25.6		-0.2	

TABLE 2
REDUCED RASTER ANALYSIS OF A
Pt-CONTAINING CHELEX STANDARD BEAD
AT 16 X 16 PIXELPOINTS

▼Original Image	▼Overlay Image	▼Threshold		INNER POINTS SRS-METHOD Mean Values c/p/s	INNER POINTS SRS-METHOD Unit Values c/p/s $nm^2 x10^{-3}$	OUTER POINTS Mean Values c/p/s	OUTER POINTS Unit Values c/p/s $nm^2/x10^{-3}$	AREA μm^2
PM	PM	17	$\bar{X}$	60.05	30.5	3.0	1.5	8.98
			SD	26.05	13.2	4.5	2.3	
PM	PM	15	$\bar{X}$	59.40	30.2	2.3	1.2	9.11
			SD	26.41	13.4	3.5	1.8	
PM	PM	11	$\bar{X}$	58.50	29.8	1.5	0.7	9.28
			SD	27.0	13.8	2.1	1.1	
				DBL-METHOD				
PT	PT	17	$\bar{X}$	42.14	21.4	7.9	4.0	9.24
			SD	12.31	6.3	5.4	2.7	
LI	PT	17	$\bar{X}$	16.48	8.4	9.5	4.8	
			SD	4.19	2.1	4.8	2.4	
RE	PT	17	$\bar{X}$	10.11	5.2	6.5	3.3	
			SD	3.7	1.9	3.1	1.5	
Calculated			$\bar{X}$	=	15.5		0.3	
PT	PT	15	$\bar{X}$	41.29	21.0	6.5	3.3	9.55
			SD	12.97	6.6	4.5	2.3	
LI	PT	15	$\bar{X}$	16.34	8.3	9.0	4.6	
			SD	4.22	2.2	4.9	2.5	
RE	PT	15	$\bar{X}$	10.07	5.1	6.0	3.1	
			SD	3.68	1.9	2.8	1.4	
Calculated			$\bar{X}$	=	15.1		0.1	
PT	PT	11	$\bar{X}$	39.86	20.3	4.4	2.3	10.0
			SD	14.16	7.2	3.6	1.8	
LI	PT	11	$\bar{X}$	16.13	8.2	7.8	4.0	
			SD	4.27	2.2	5.1	2.6	
RE	PT	11	$\bar{X}$	9.94	5.1	5.5	2.8	
			SD	3.70	1.9	2.5	1.2	
Calculated			$\bar{X}$	=	14.5		-0.8	
PT	PM	17	$\bar{X}$	42.66	21.7	10.5	5.3	8.94
			SD	12.25	6.3	7.9	4.0	
LI	PM	17	$\bar{X}$	16.33	8.3	10.8	5.5	
			SD	4.21	2.1	5.8	3.0	
RE	PM	17	$\bar{X}$	10.00	5.1	7.3	3.7	
			SD	3.74	1.9	3.6	1.8	
Calculated			$\bar{X}$	=	15.8		1.1	
PT	PM	15	$\bar{X}$	42.31	21.5	9.9	5.1	9.07
			SD	12.50	6.4	7.8	4.0	
LI	PM	15	$\bar{X}$	16.30	8.3	10.6	5.4	
			SD	4.20	2.1	5.9	3.0	
RE	PM	15	$\bar{X}$	10.00	5.1	7.2	3.6	
			SD	3.71	1.9	3.6	1.8	
Calculated			$\bar{X}$	=	15.7		1.0	
PT	PM	11	$\bar{X}$	41.88	21.3	9.1	4.6	9.29
			SD	12.82	6.5	7.1	3.6	
LI	PM	11	$\bar{X}$	16.27	8.3	10.3	5.2	
			SD	4.28	2.2	5.6	2.9	
RE	PM	11	$\bar{X}$	9.98	5.1	7.0	3.6	
			SD	3.69	1.9	3.7	1.9	
Calculated			$\bar{X}$	=	15.5		0.6	

compared to the DBL-method around the Pt-Lα region (see Fig. 1). The four arrays are given in Figs. 7-10. In Fig. 7, the Pt-Mα array is given (indicated as PM), in which the special background region (Bgr*) on line is substracted (SRS-method). The (PM) threshold 15 c/p/s overlay is superimposed. In Fig. 8 the array of the Pt-Lα minus background region zero is given (indicated as PT), with a threshold of 15 c/p/s overlay. In Figs. 10 and 11 the pseudo-peak region arrays LI and RE both with the virtually empty zero background region

ORIGINAL IMAGE:XRAY PM
OVERLAY IMAGE:XRAY PM OVERLAY THRESHOLD:109
MAGNIFICATION: 62464 TOTAL AREA: 4004611 NM^2
LABEL:ACIDOPHIL GRAN 4 2-1-1985 XRAY

NUMBER OF POINTS(I P):113 NUMBER OF POINTS(O P):143
MEAN (I P):136.69 C/P MEAN (O P): 68.60 C/P
S. DEVIATION (I P): 18.50 C/P S. DEVIATION (O P): 22.56 C/P
MEAN+2S.D.(I P): 173.71 C/P MEAN+2S.D.(O P): 113.74 C/P
DEGREES OF FREEDOM: 254 T-VALUE: 68.09 P ≤ 0.05
DWELL-TIME/POINT: 1000000 USEC.
SPOTAREA: 1963 NM^2 ANALYZED AREA 12.55 %
INTER PIXEL DISTANCE: 125 NM AREA(I P): 1767660 NM^2
[XRAY PM]= 6.96E-02 C/P/S/NM^2
[S. DEVIATION]= 9.42E-03 C/P/S/NM^2 C.V.= 13.53 % **SRS**

	86	62	123	150	114	152	158	144	142	131	119	103	62	84	75	64
	95	114	103	161	142	121	147	160	187	139	130	99	119	98	79	52
	87	100	119	145	155	116	135	155	171	164	159	135	91	88	83	65
	107	116	139	141	95	124	131	156	174	165	179	133	110	98	83	77
	79	135	135	120	127	133	146	146	174	187	167	129	130	104	75	65
	107	126	151	142	155	127	142	149	139	172	150	153	131	100	79	57
	103	122	158	137	123	114	131	112	111	151	138	112	138	102	66	19
	67	99	115	127	110	121	107	126	130	148	151	163	143	109	70	44
	87	101	111	110	123	122	127	86	131	157	142	151	138	108	67	26
	54	74	131	113	63	123	87	96	118	116	119	130	146	64	51	34
	30	55	82	96	127	96	103	85	111	124	139	146	87	74	51	36
	54	50	59	54	47	82	86	103	114	133	86	93	114	75	58	43
	46	39	50	27	27	36	74	89	86	83	94	70	95	77	54	29
	58	70	50	69	58	69	78	98	31	52	54	88	67	65	55	32
	47	42	23	53	43	83	59	67	47	84	59	64	102	51	62	27
11	46	31	46	45	67	52	51	57	46	59	47	56	51	74	74	64

Fig. 11. Reduced raster array from an eosinophilic granule in cross section. Pt-Mα array (minus background*), with threshold 109 superimposed. SRS-method.

ORIGINAL IMAGE:XRAY PT
OVERLAY IMAGE:XRAY PM OVERLAY THRESHOLD:109
MAGNIFICATION: 62464 TOTAL AREA: 4004611 NM^2
LABEL:ACIDOPHIL GRAN 4 2-1-1985 XRAY

NUMBER OF POINTS(I P):113 NUMBER OF POINTS(O P):143
MEAN (I P): 76.62 C/P MEAN (O P): 41.69 C/P
S. DEVIATION (I P): 11.51 C/P S. DEVIATION (O P): 16.18 C/P
MEAN+2S.D.(I P): 99.65 C/P MEAN+2S.D.(O P): 74.07 C/P
DEGREES OF FREEDOM: 254 T-VALUE: 34.92 P ≤ 0.05
DWELL-TIME/POINT: 1000000 USEC.
SPOTAREA: 1963 NM^2 ANALYZED AREA 12.55 %
INTER PIXEL DISTANCE: 125 NM AREA(I P): 1767660 NM^2
[XRAY PT]= 3.90E-02 C/P/S/NM^2
[S. DEVIATION]= 5.86E-03 C/P/S/NM^2 C.V.= 15.02 % **DBL**

	58	40	75	61	76	74	78	89	62	75	62	57	45	52	48	17
	64	73	64	97	66	92	73	91	77	84	66	55	51	56	52	21
	69	74	71	81	60	86	69	82	102	88	71	74	59	45	51	14
	71	67	87	72	78	77	71	88	90	92	91	65	83	55	59	12
	62	80	75	78	74	80	71	94	66	96	94	62	67	48	42	16
	55	74	86	82	74	72	66	83	87	91	95	80	71	56	50	10
	70	62	78	82	70	89	70	88	90	107	106	78	74	63	54	8
	54	71	63	62	75	83	59	78	83	69	90	92	63	79	35	16
	42	54	78	75	74	65	66	74	75	69	90	92	70	58	30	10
	43	48	55	69	51	53	62	69	79	57	82	77	75	57	39	15
	35	39	38	44	62	64	50	63	75	57	74	73	70	47	19	14
	38	41	34	35	39	67	54	49	78	66	83	39	55	31	26	11
	34	41	30	34	31	32	43	44	54	52	54	39	50	32	27	12
	30	35	38	50	43	45	31	32	42	41	30	39	39	32	35	4
	35	29	39	23	46	39	42	43	39	44	47	37	38	33	34	10
12	26	30	30	44	35	33	39	38	46	45	34	37	35	37	26	8

Fig. 12. Reduced raster array from the same granule in cross section. Pt-Lα array (minus background Zero). The PM-threshold applied in Fig. 11 is also superimposed here. DBL-method.

ORIGINAL IMAGE:XRAY LI
OVERLAY IMAGE:XRAY PM OVERLAY THRESHOLD:109
MAGNIFICATION: 62464 TOTAL AREA: 4004611 NM^2
LABEL:ACIDOPHIL GRAN 4 2-1-1985 XRAY

NUMBER OF POINTS(I P):113 NUMBER OF POINTS(O P):143
MEAN (I P): 20.46 C/P MEAN (O P): 16.30 C/P
S. DEVIATION (I P): 4.70 C/P S. DEVIATION (O P): 5.17 C/P
MEAN+2S.D.(I P): 29.88 C/P MEAN+2S.D.(O P): 26.66 C/P
DEGREES OF FREEDOM: 254 T-VALUE: 4.16 P ≤ 0.05
DWELL-TIME/POINT: 1000000 USEC.
SPOTAREA: 1963 NM^2 ANALYZED AREA 12.55 %
INTER PIXEL DISTANCE: 125 NM AREA(I P): 1767660 NM^2
[XRAY LI]= 1.04E-02 C/P/S/NM^2
[S. DEVIATION]= 2.39E-03 C/P/S/NM^2 C.V.= 23.00 %

	18	13	14	12	23	23	18	19	23	13	22	19	15	12	23	9
	19	16	19	21	31	23	18	29	19	19	18	20	30	14	11	13
	19	12	22	12	23	13	18	21	22	12	23	28	26	21	11	18
	18	18	23	24	23	19	22	27	27	17	19	20	22	13	7	12
	27	29	18	25	14	22	22	20	22	13	26	22	18	16	14	9
	14	24	26	18	18	21	23	18	27	22	27	21	27	9	18	18
	19	21	23	25	22	17	14	16	31	25	15	18	15	30	19	8
	18	13	23	23	22	18	30	29	15	17	30	13	26	16	15	9
	22	21	22	20	14	21	18	30	19	24	27	22	14	17	18	15
	10	16	11	22	23	18	23	16	14	17	22	22	14	22	23	4
	22	16	14	12	23	19	14	15	22	12	19	17	15	18	7	9
	14	16	18	13	19	16	30	11	22	22	26	16	15	8	18	9
	18	18	19	20	23	17	18	12	18	15	11	19	14	20	18	15
	19	17	19	18	15	18	19	16	23	24	10	15	10	16	18	8
	10	17	18	11	15	9	15	16	15	15	19	15	22	22	18	5
13	22	18	19	20	11	16	26	14	15	17	10	8	18	11	10	8

Fig. 13. Reduced raster array from the same granule in cross section, with the same PM threshold 109 superimposed. Background LI (minus background Zero). Used for DBL method. (see Fig. 6).

ORIGINAL IMAGE:XRAY RE
OVERLAY IMAGE:XRAY PM OVERLAY THRESHOLD:109
MAGNIFICATION: 62464 TOTAL AREA: 4004611 NM^2
LABEL:ACIDOPHIL GRAN 4 2-1-1985 XRAY

NUMBER OF POINTS(I P):113 NUMBER OF POINTS(O P):143
MEAN (I P): 12.76 C/P MEAN (O P): 10.07 C/P
S. DEVIATION (I P): 3.56 C/P S. DEVIATION (O P): 4.00 C/P
MEAN+2S.D.(I P): 19.88 C/P MEAN+2S.D.(O P): 18.09 C/P
DEGREES OF FREEDOM: 254 T-VALUE: 2.68 P ≤ 0.05
DWELL-TIME/POINT: 1000000 USEC.
SPOTAREA: 1963 NM^2 ANALYZED AREA 12.55 %
INTER PIXEL DISTANCE: 125 NM AREA(I P): 1767660 NM^2
[XRAY RE]= 6.49E-03 C/P/S/NM^2
[S. DEVIATION]= 1.81E-03 C/P/S/NM^2 C.V.= 27.92 %

	11	8	14	11	14	9	11	13	10	16	7	14	7	14	7	12
	14	14	7	17	14	19	7	13	11	15	11	8	14	3	14	5
	14	1	11	7	15	14	14	11	11	9	14	11	7	7	6	6
	14	13	15	16	22	11	15	6	15	13	14	9	11	8	15	10
	18	10	19	13	14	11	7	16	18	13	14	17	10	7	15	10
	11	12	11	10	10	10	11	21	10	14	19	14	10	10	6	13
	10	7	15	14	14	7	10	13	10	20	14	10	15	15	11	8
	10	8	10	5	14	7	6	15	7	11	15	17	11	14	14	11
	15	8	19	17	10	6	14	10	11	10	14	12	14	13	14	7
	11	12	15	23	19	19	19	13	15	11	19	15	10	6	19	6
	14	11	14	8	14	8	10	3	7	11	18	17	14	9	7	7
	10	9	11	4	14	7	19	11	14	8	7	11	15	8	10	9
	11	4	7	0	6	5	11	14	15	10	7	7	11	14	11	13
	7	10	14	12	14	8	11	12	18	12	10	4	6	8	15	7
	18	10	10	5	6	4	14	5	7	9	11	15	14	8	3	16
14	10	6	14	12	6	8	7	4	11	11	11	8	6	11	11	12

Fig. 14. Reduced raster array from the same granule in cross section, with the same threshold 109 superimposed. Background region RE (minus background Zero). Used for DBL method (see Fig. 6).

TABLE 3
REDUCED RASTER ANALYSIS OF AN EOSINOPHILIC GRANULE AT 16 X 16 PIXELPOINTS

▼Original Image	▼Overlay Image	▼Threshold		INNER POINTS Mean Values c/p/s	INNER POINTS Unit Values c/p/s nm^{2}x10^{-3}	OUTER POINTS Mean Values c/p/s	OUTER POINTS Unit Values c/p/s nm^{2}x10^{-3}	AREA µm2
				SRS-METHOD				
PM	PM	109	$\bar{X}$	136.69	69.6	68.6	35.1	1.77
			SD	18.5	9.4	22.6	11.4	
PM	PM	113	$\bar{X}$	138.95	70.7	71.1	36.2	1.63
			SD	17.54	8.9	24.1	12.3	
				DBL-METHOD				
PT	PT	73	$\bar{X}$	82.80	42.1	46.1	23.5	1.20
			SD	8.24	4.2	17.0	8.7	
LI	PT	73	$\bar{X}$	20.51	10.4	17.1	8.7	
			SD	5.01	2.6	5.2	2.7	
RE	PT	73	$\bar{X}$	12.94	6.6	10.5	5.4	
			SD	3.85	2.0	3.9	2.0	
Calculated			$\bar{X}$	=	34.6		17.3	
PT	PM	109	$\bar{X}$	76.62	39.0	41.4	21.2	
			SD	11.51	5.9	16.2	8.3	
LI	PM	109	$\bar{X}$	20.46	10.4	16.3	8.3	1.77
			SD	4.70	2.4	5.2	2.6	
RE	PM	109	$\bar{X}$	12.76	6.5	10.1	5.1	
			SD	3.56	1.8	4.0	2.0	
Calculated			$\bar{X}$	=	31.5		15.3	

subtracted on line as before are shown with the (PT) threshold Pt-Lα 15 c/p/s superimposed to delineate the Chelex bead from the surrounding Epon, devoid of Pt. The mean net-intensity "inside" and "outside" values are calculated and the background under the Pt-Lα reconstructed in the same way as outlined before and the results are collected in Table 2. For the SRS-method presented in the first horizontal row, the Pt-Mα "inside" mean net-intensity values are twice as high as the same type of value obtained by the DBL-method. The "outside"-mean net-intensity values are both close to zero, (1.5 to 0.7 x 10^{-3} and -0.8 to 1.0 x 10^{-3} c/p/s/nm^2 respectively). When, in order to reconstruct the background under the Pt-Lα region by the DBL-method different threshold values are superimposed over the pseudo-peak LI and RE arrays, other mean net-intensity "inside/outside" values are obtained. These values are also given in Table 2. The main conclusion, however, is not affected by this. Moreover, as will be shown, these differences are cancelled out in the final calculation. The same set of conditions is used to measure the Pt concentration in a set of granules from an eosinophilic granulocyte present in the same ultrathin section, in which the peroxidase activity is also cytochemically converted into a Pt-containing reaction product. The four arrays are shown in Figs. 11-14, with threshold overlays, set to delineate the granule from the surrounding (Pt-containing) cytoplasm. The results of the "inside/outside" mean net-intensity

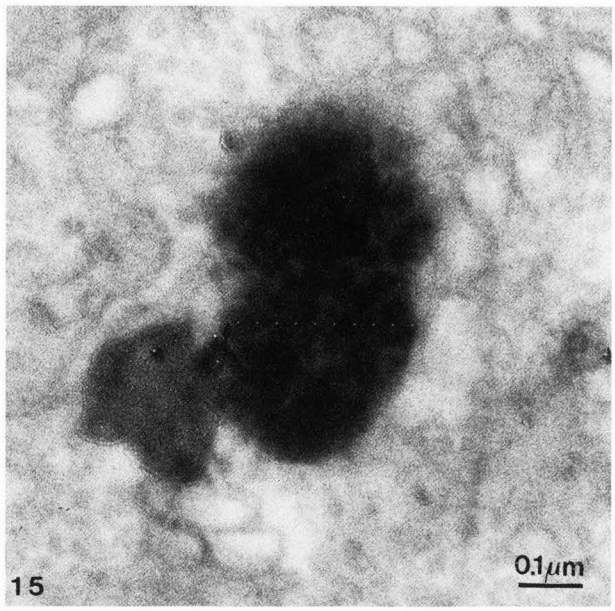

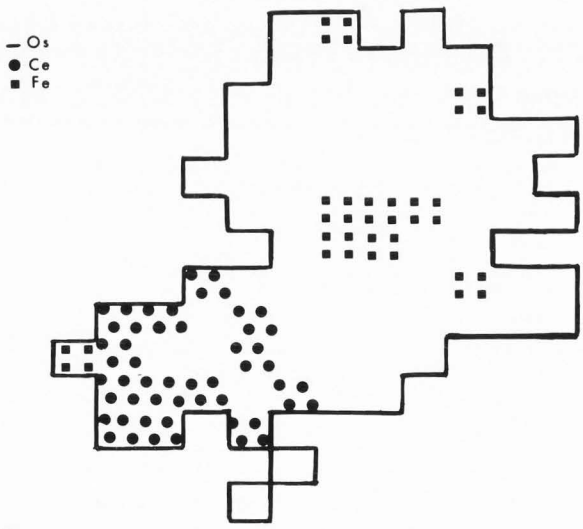

16

Figs. 15 and 16. In Fig. 15 the transmission electron miscroscopic image of a human liver lysosome containing stored ferritin particles and cerium precipitate from the acid phosphatase reaction is shown. In the post-fixed tissue the precise element-loci were unknown. A reduced raster analysis of the area including: Fe,Ce,Os was performed, and in each array a threshold was introduced, delineating the element from its surroundings. In the printing process the figures in the array were defaulted, so only the overlay is printed. The three overlay figures were subsequently superimposed giving the precise elemental loci in the lysosome(s) (Fig. 16).

calculations for the SRS and DBL method, as outlined before, are given in Table 3.

For the SRS method the Pt-Mα "inside" mean net-intensity value (69.6 x 10^{-3} c/p/s/nm^2) is about twice the "outside" mean net-intensity value (35.1 x 10^{-3} c/p/s/nm^2). For the DBL-method the Pt-Lα "inside/outside" ratio is also about 2, depending on the threshold values superimposed in the arrays. Since the absolute Pt concentration in the Chelex beads is known (18.3% w/w), the c/p/s/nm^2-values for the granule can be converted into the absolute concentration values. The Pt-Lα and Pt-Mα threshold gave about the same final results irrespective whether the SRS or the DBL-method was used. These values are collected in Table 4, for the various threshold and conditions (SRS- and DBL) chosen for both regions.

TABLE 4
ABSOLUTE Pt-CONCENTRATION IN THE EOSINOPHILIC GRANULE AND CYTOPLASM. REDUCED RASTER MODE AT 16 X 16 PIXELPOINTS

SRS-METHOD AROUND Pt-Mα (PM)
(Unit values: x 10^{-3} c/p/s/nm^2)

	GRANULE (inner points)	
Threshold	109	113
Mean values	69.6	70.7
Standard PM/PM-17 = 30.5	41.8% w/w	42.4% w/w
,, PM/PM-15 = 30.2	42.2% ,,	42.8% ,,
,, PM/PM-11 = 29.8	42.7% ,,	43.4% ,,
	CYTOPLASM (outer points)	
Standard PM/PM-17 = 30.5	21.1% w/w	21.7% w/w
,, PM/PM-15 = 30.2	21.3% ,,	21.9% ,,
,, PM/PM-11 = 29.8	21.6% ,,	22.3% ,,

DBL-METHOD AROUND Pt-Lα (PT)

	GRANULE		CYTOPLASM	
Thresholds	109	73	109	73
Mean values	31.5	34.6	15.3	17.3
	% w/w			
Standard PT/PT-17=15.5	37.2	40.9	18.1	20.4
,, PT/PT-15=15.1	38.2	41.9	18.5	21.0
,, PT/PT-11=14.5	39.8	43.7	19.3	21.8
Standard PT/PM-17=15.8	36.5	40.1	17.7	20.0
,, PT/PM-15=15.7	36.7	40.3	17.8	20.2
,, PT/PM-11=15.5	37.2	40.9	18.1	20.4

Mα (SRS):Lα(DBL) ratio = PM/PM-17:PT/PM-17 = 1.9:1
(of the standard) PM/PM-15:PT/PM-15 = 1.9:1
PM/PM-11:PT/PM-11 = 1.9:1

From the results the following conclusions can be formulated:
1. When the "standard" and the "unknown" are measured strictly under the same conditions and the reduced raster arrays are deconvoluted according to the same method, the absolute concentration value calculated, is not different.
2. The threshold values chosen to delineate the particle do influence the final result, but again this influence is very small.
3. The "outside" concentration values can be kept low when the outside region does not contain the element of interest, as demonstrated by the Epon surrounded erythrocyte and Chelex.
4. The cytoplasmic Pt-values are rather alike irrespective of the deconvolution procedure applied to the reduced raster arrays obtained.

Provided the calculations, now performed off-line by hand, can be introduced into the computer program, and these calculations can be performed in the time available during the acquisition on-line, the DBL method is to be preferred. However, the SRS-method applied up to now, when carefully conditioned, can produce absolute values identical to the DBL values.

Homogeneity of the Chelex Pt-standards

In this connection the homogeneity of the Chelex standard material, in this case loaded with Pt, can be established. With a constant spot size and beam intensity, the area analysed in the reduced raster was increased, while the mean Pt net-intensity value of 16 x 16 pixelpoints is collected at each magnification. In Table 5, the Pt-Mα values are compared with the percentage of the total area that was analysed, and related to the interpixel distance (IPD). When the IPD is smaller than the spot size, the lowest mean Pt net-intensity is measured, the value of which increases signficantly, till about 1/4 of the screen is covered with the 16 x 16 pixelpoints. The standard deviation varies in an alternating way (coefficient of variance = CV = 35-71%). Whenever the standard is measured at about the same interpixel distance as the "unknown", the variation present may cancel out. In Table 6 the mean values obtained by the DBL-method are compared with those obtained by the SRS-method. Probably due to a more careful selection of the part of the Chelex standard bead, the differences are not significant here and hence the standards are homogeneously loaded. The ratio SRS/DBL is rather constant.

Comparison of the reduced raster results to the point analysis results

In Table 7 the mean SRS and DBL values of the reduced raster mode are compared with the concomitantly obtained point analysis values deconvoluted in the same way. The ratios obtained between the reduced raster and point analysis values are rather constant.

Cerium and iron distribution in liver parenchymal lysosomes in iron storage diseases

The integrated morphometrical and chemical analysis is designed to enable heteromorphic heterogenic cell organelles to be analysed quantitatively. This was explored in a small lysosomal population in a human liver parenchymal cell.

In unstained ultrathin sections of such liver parenchymal cells from a patient with an iron storage disease, after flebotomy, several irregular shaped large electron-dense areas are present (Figs. 15-17). The acid phosphatase activity, qualitatively illustrated the lysosomal character of the electron dense bodies by the presence of the capture-element cerium, used to precipitate the phosphate liberated by the enzyme action. In addition, the iron of the stored ferritin is present. Three types of lysosomal bodies can be distinguished in this way:
1. lysosomes, containing only cerium (primary lysosomes),
2. lysosomal bodies, containing only iron (ferritin storage vacuoles/residual body), and

TABLE 5
CHELEX Pt-STANDARD-BEADS IN CROSS-SECTION
ANALYSED BY THE REDUCED RASTER MODE AT
VARIOUS MAGNIFICATIONS AND 50 nm SPOT SIZE

SRS-METHOD

Magnification	Mean Value c/p/s	Unit Value c/p/s nm^2 x 10^{-3}	CV %	Total Area μm^2	Analysed Area %	IPD nm	p-value
204,800	17.71	9.1		0.37	135	38	
			38				<0.40
SD	6.7	3.4					
126,030	19.70	10.1		1.00	51		
			67			62	<0.01
SD	13.11	6.7					
65,536	21.67	11.1		3.64	14	119	
			35				<0.05
SD	7.6	3.9					
51,200	23.91	12.3		5.96	8	159	
			46				<0.05
SD	11.0	5.6					
25,600	30.17	15.4		23.8	2	305	
			71				
SD	21.5	11.0					

TABLE 6
CHELEX Pt-STANDARD-BEADS IN CROSS-SECTION
ANALYSED BY REDUCED RASTER MODE AT
TWO MAGNIFICATIONS AND SPOT SIZES

Magnification	Mα SRS-METHOD Inner c/p/s/nm^2x10^{-3}	Outer	CV	Lα DBL-METHOD Inner c/p/s/nm^2x10^{-3}	Outer	Mα/Lα ratio
12,800	10.9	0.2	27	5.8	0.0	1.9
SD	3.0	0.2		0.7		
100 nm p-val.		> 0.40				
12,800	14.6	0.7	38	7.6	0.0	1.9
SD	5.5	0.6		1.3		
50 nm p-val.		> 0.05				
25,600	14.0	0.8	39	7.9	0.0	1.8
SD	5.5	0.8		1.2		
50 nm p-val.		> 0.05				

3. lysosomes, containing both cerium and iron (secondary lysosomes). In Figs. 15 and 16 it is demonstrated how, by the application of the reduced raster method, the inhomogeneously distributed elements within one lysosome, can be differentiated, and related to the presence of a third element, osmium, which delineates the lysosome from the cytoplasmic surrounding.

Six lysosomal structures within one liver parenchymal cell were analysed by the reduced raster method (Fig. 17). Iron-containing Chelex standard beads with a known iron concentration of 11.2% w/w were present in the periphery of the tissue in the same ultrathin section. In Table 8, the measured cerium mean net-intensities (SRS-method), converted into unit values (c/p/s/nm^2), are listed. From these values the following conclusions can be drawn:

1) The cerium, present in all lysosomes analysed, is rather homogeneously distributed over the lysosomal area (CV: 17-30%) and rather small mutual variations of it are present between the various lysosomal structures (CV: 13%).
2) Over the same lysosomes the iron is distributed much more inhomogeneously (CV: 54-58%) and the differences between the lysosomes is high (CV = 91%). One small lysosome was considered to be a primary lysosome, containing no iron.
3) The cytoplasmic ("outside" the particle) areas contain mean net-intensities for both the cerium and iron which are very low, though present and rather consistent. The "inside" mean net-intensity values for both the cerium and the iron were significantly different from the values present "outside" the lysosomal structures.
4) The absolute iron concentration is between 7 and 55 % w/w.
5) The area occupied by both the cerium and the iron are calculated. In some lysosomes, iron and cerium are present, occupying the same area, in other lysosomes there are different areas involved.

Discussion

The integrated morphometrical and chemical analysis method is designed to enable the analysis of heteromorph-heterogenic cellular organelles in ultrathin sections, like lysosomes and particles, which, by cytochemical reaction, are well differentiated from their cytoplasmic surroundings. The presence of Chelex standard beads, loaded with a known amount of the element of interest, in the same ultrathin section assists one in the quantification of the elements present in cellular organelles to be analysed. The analytical method is rather straight forward. A small (reduced) raster is located around the particle to be analysed. A matrix of a fixed number of points is, at equidistances, divided over that reduced raster area, and the information (collected from any of the detectors available) is sampled during a constant dwell time of the beam at each point. The digitalized information is presented as an array of figures. Like the information collected in (multiple) point analysis, the information from "inside" the particle is to be compared with that from the "outside" the particle area within the reduced raster. To separate the "inside" and "outside" information a threshold value has to be chosen, and once introduced, the computer delineates the points in the array having a value over and under the value selected. The morphometrical information is obtained by relating the number of points "inside" the delineation to the total numbers present in the reduced raster array. When the array comprises digitalized information from the X-ray detector, the mean value of the digitalized information is given for all the points "inside" and "outside" the chosen delineation. This mean value can be converted into unit values

TABLE 7
CHELEX Pt-STANDARD-BEADS IN CROSS-SECTION ANALYSED BY REDUCED RASTER MODE AND COMPARED WITH SINGLE POINT ANALYSIS

Spot Size nm	SRS-METHOD Red. Raster c/p/s/nm^2 x 10^{-3}	Point Analysis c/p/s/nm^2 x 10^{-3}	Ratio Red. Rast.: Point	DBL-METHOD Red. Raster c/p/s/nm^2 x 10^{-3}	Point Analysis c/p/s/nm^2 x 10^{-3}	Ratio Red. Rast.: Point
100	10.88	28.46	38:100	5.75	16.49	35:100
50	14.62	37.30	39:100	7.62	22.83	33:100
50	14.02	37.30	38:100	7.98	22.83	35.100
Mα (SRS):Lα (DBL) ratio =				10.88 : 5.75 = 1.9 : 1		
				14.62 : 7.62 = 1.9 : 1		
				14.02 : 7.98 = 1.8 : 1		

(counts/pixelpoint/sec/nm^2 irradiated) and as similar information is obtained from the co-embedded standard in the same ultrathin section, absolute mean concentrations can be obtained. As any figure can be introduced as a threshold into the arrays, local elemental concentrations within a single particle can be monitored. Whereas delineations obtained in one (elemental) array can be superimposed over three additional elemental arrays, obtained simultaneously, to relate the elements mutually (Figs. 15 and 16).

Much of the reliability of the chemical information obtained by the X-ray detector is determined by the deconvolution methods applied, to obtain the net-intensity values per point. Not all the deconvolution methods commonly available for point analyses were considered applicable for the on-line analysis. As net-intensity values were the aim of the method, the program was designed to subtract a single background region from the, generally in 1 sec acquired, peak region of interest (Single Region Subtraction method). Initially two options were proposed for the background region to be subtracted from the peak region: 1) a zero-region between 0.200 and 0.400 keV according to the method proposed by Shuman et al. (10) leading to (net)-intensity values with a so-called "gross" character, 2) a region anywhere in the peak-free background of the spectrum. When, in a later phase that background region was subtracted from the peak region to be deconvoluted, the resulting net-intensity value was approximately similar to the value obtained from a complete 100 sec point analysis spectrum deconvoluted according to the "filter method" routinely present in the Tracor/Northern 2000 software. (This method was suggested by R. Lampers and Mrs. C.J. G. Blok-van Hoek, Tracor Europe). The possibility to subtract two background regions (DBL-method), originally present in the T/N program IPP, was considered not to be applicable to the on-line procedure. This is still the case, but the

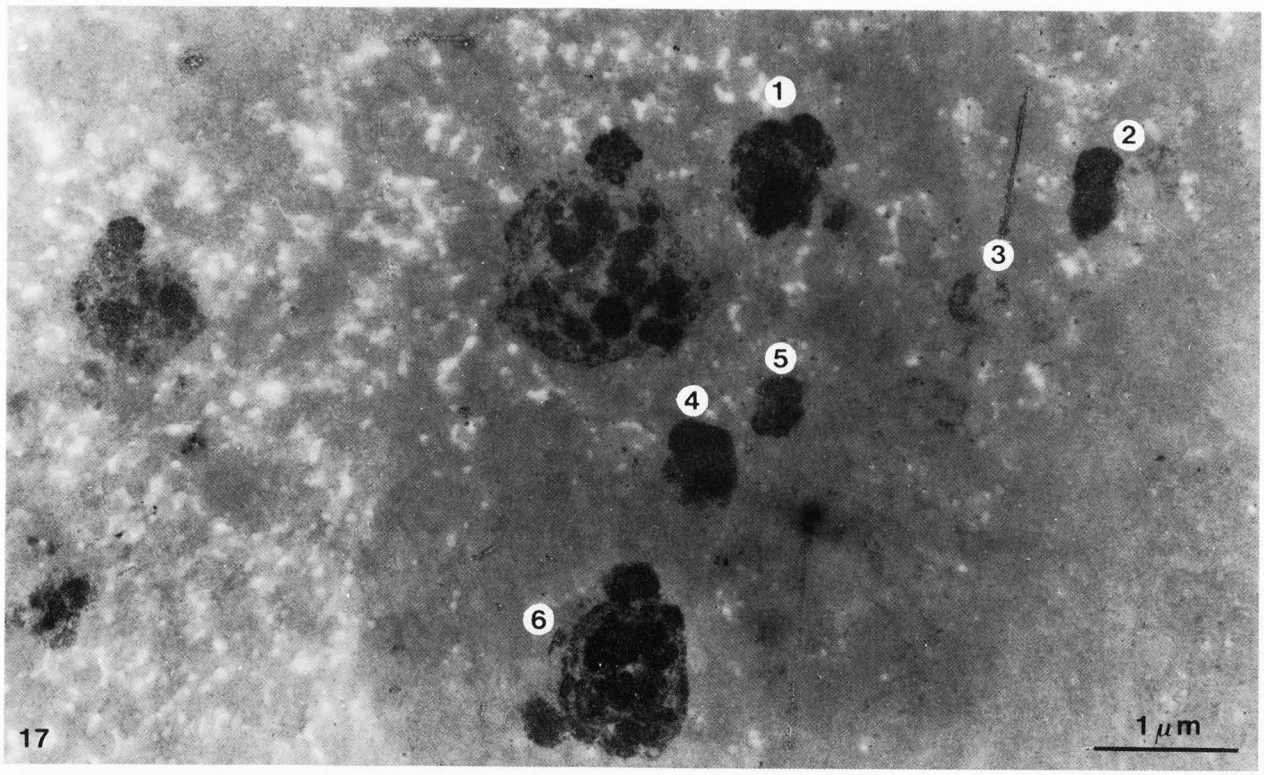

Fig. 17. Transmission electron microscopic image of the area of a human liver section, including cerium and iron-containing lysosomes as shown in Figs. 15 & 16. The lysosomes marked 1 to 6 are analysed by reduced raster, using the SRS-deconvolution. The results are collected in Table 8.

TABLE 8
LYSOSOMES IN HUMAN LIVER SECTIONS ANALYSED BY REDUCED RASTER MODE AT 16 X 16 PIXELPOINTS SRS-METHOD

CERIUM			IRON		
Inner Points	Outer Points	Area	Inner Points	Outer Points	Area
c/p/s/nm^2 x 10^{-3}		μm^2	c/p/s/nm^2 x 10^{-3}		μm^2
Lys 1					
$\bar{X}$= 374	$\bar{X}$= 62		$\bar{X}$= 139	$\bar{X}$= 11	
SD= 88	SD= 43	0.291	SD= 75	SD= 14	0.179
CV= 23%	CV= 69%		CV= 54%	CV= -	
Lys 2					
$\bar{X}$= 315	$\bar{X}$= 64		$\bar{X}$= 0	$\bar{X}$= 15	
SD= 78	SD= 39	0.110	SD= -	SD= 31	-
CV= 25%	CV= 61%		CV= -	CV= -	
Lys 3					
$\bar{X}$= 289	$\bar{X}$= 64		$\bar{X}$= 67	$\bar{X}$= 15	
SD= 58	SD= 39	0.064	SD= -	SD= 31	0.01
CV= 20%	CV= 61%		CV= -	CV= -	
Lys 4					
$\bar{X}$= 273	$\bar{X}$= 82		$\bar{X}$= 161	$\bar{X}$= 16	
SD= 46	SD= 44	0.083	X=SD=93	SD= 16	0.083
CV= 17%	CV= 54%		CV= 58%	CV=100%	
Lys 5					
$\bar{X}$= 289	$\bar{X}$= 82		$\bar{X}$= 194	$\bar{X}$= 16	
SD= 88	SD= 44	0.052	SD=112	SD= 16	0.069
CV= 30%	CV= 54%		CV= 58%	CV=100%	
Lys 6					
$\bar{X}$= 355	$\bar{X}$= 93		$\bar{X}$= 599	$\bar{X}$= 16	
SD= 72	SD= 39	0.403	SD=325	SD= 16	0.491
CV= 20%	CV= 42%		CV= 54%	CV=100%	

Total lysosomal population
Lysosomes:
Cerium: 315 +/- 40.0 x 10^{-3} c/p/s/nm^2; CV = 13%
Iron : 232 +/- 210 x 10^{-3} c/p/s/nm^2; CV = 91%
Cytoplasm:
Cerium: 75 +/- 13 x 10^{-3} c/p/s/nm^2; CV = 17%
Iron : 15 +/- 2 x 10^{-3} c/p/s/nm^2; CV = 13%

---

off-line procedure outlined now enables one to judge the results whenever introduction can be realized. It leads the way in the steps the computer has to take to be able to perform the DBL-method "on-line". In the first experiment the erythrocyte, known to be only surrounded by Epon, was analysed to compare the SRS- with the DBL-method, with the Pt-Lα as the elemental peak of choice. For the SRS-method the content of the background pseudopeak LI was used to be subtracted. The "inside" values when converted into unit values, were more or less identical in both methods (23.6, 23.6 and 23.0 and 24.7 x 10^{-3} c/p/s/nm^2) but the DBL-"outside" values were much closer to reality, viz., no platinum present in the Epon, than the SRS-method ("outside" = 0.8 - 1.0 vs. 0.4 - 0.0 x 10^{-3} c/p/s/nm^2.

In the second experiment, the Chelex Pt-standard was also analysed with the condition that no platinum should be present in the surrounding Epon. Now the SRS-method for the Mα-region of the spectrum (and a single peak-free region, between 1.240 and 1.640 keV) was compared to the DBL-method around the Pt-Lα used in experiment 1. In addition, the influence of the various threshold settings was estimated for the DBL-method. The Pt-Mα peak deconvoluted with the SRS-method gave Pt-net-intensity unit values for the "inside" area (30.5 x 10^{-3} c/p/s/nm^2) of about twice the Pt-Lα peak value, deconvoluted with the DBL-method (15.0 x 10^{-3} c/p/s/nm^2). The "outside" values were 1.5 x 10^{-3} c/p/s/nm^2 for the SRS- and between -0.8 to 1.1 x 10^{-3} c/p/s/nm^2 for the DBL-method. The threshold values in the arrays were chosen subjectively. Considering the mean "outer particle" values obtained after that subjective decision, it turned out that the mean "outside" c/p/s-value plus two times the standard deviation resulted in a figure close to the value which has been selected subjectively before as a threshold for the transition from Epon to cytoplasm. (Threshold = $\bar{X}$(OP) + 2 SD(OP) (in which = $\bar{X}$(OP) = mean "outer" net-intensity value, SD = the standard deviation of the mean for the "outer"points).

In the third experiment (with the same deconvolution set-up as in the second experiment), platinum-containing eosinophilic granules present in a platinum-containing cytoplasm, were analysed by the same two methods. In this case too the Pt-Mα-related results according to the SRS-method were again two times higher than the concomitantly acquired unit values from the Pt-Lα-centered DBL-method, for both the "inside" and "outside" parts of the reduced raster area. Moreover, considered ad hoc, the Pt Lα and Mα mean "outside" c/p/s value (= actually cytoplasm) plus two times the standard deviation value appeared to be close to the threshold value chosen before to delineate the particle from the cytoplasm on subjective criteria. The results of the three experiments are summarized in Table 4. As the acquisition of the Chelex Pt-bead cross section was performed under the same instrumental conditions (apart from the beam-intensity at the actual moments of analysis), the mean unit values of the Chelex standard beads can be related to those of the eosinophilic granule taken as an example in experiment three (Tables 3 and 4). In that way the relative differences between the two deconvolution methods (SRS/Pt-Mα) and DBL/Pt-Lα) were judged. From the conversion into absolute values, shown in Table 4, it is clear that both methods end up with the same absolute concentrations. Moreover, the influence of the various threshold settings in the DBL-method is also rather minimal.

The results collected in Table 4 also indicate that the aim to have a significant difference between the particle and its immediate surroundings (viz., between the "inside" and "outside" part of the reduced raster analysed) from the statistical point of view is valid and the first rule to be obeyed. In practice the condition: $\bar{X}$(OP) + 2 SD(OP) < $\bar{X}$(IP) sets the limit to the application of the method, when for one reason or another, the cytoplasmic elemental concentrations are rather high.

The presence of pseudo-elemental peak regions representing continuum parts of the spectrum can be used to monitor the mass-differences. In Figs.

4,5,9 and 10, representing the background regions LI and RE in the two specimens analyzed, the areas (delineated by the Pt-Lα or Mα thresholds), can be compared for the "inside" and "outside" mean "mass-related" values when converted into unit values. The "p-values" are given in the top captions for the relevant comparisons, tested, indicating a significant higher local mass inside the delineated areas than in the Epon surroundings.

With respect to homogeneity of the obtained Chelex Pt-information the two types of experiments performed (variation in magnification at constant diameter and with variable spot diameter) gave about the same results. There is an unexpected relation between the magnification of the STEM-mode image employed (25,000 to 205,000 x) and the mean Pt-value measured (Table 5). This might be due to elements in the bead or to the inhomogeneous conditions in the electronmicroscopic configuration at the various magnifications. The results of the second experiment (Table 6) gave a similar set of unit values for the two magnifications and spot sizes tested, be it with more acceptable standard deviation values for the lowest magnifications than in the first experiment of this kind.

The values are given for better or for worse. The presence of the high silicon peak in this spectrum indicates that better conditions might improve the coefficients of variance, now obtained with these ultrathin sections. In Table 7, the concomitantly acquired point analysis values for the Chelex Pt-standard are given (converted into unit values) which can be related to the values obtained with the reduced raster mode under the same conditions shown in Table 6. The ratio between the mean values obtained by the reduced raster method and those from the point analysis of this homogeneous object is rather constant for both deconvolution modes.

The information collected in Table 8 is an attempt to obtain localized quantitative elemental information from two elements present in one lysosome (viz., iron and cerium). A population of heteromorphic, heterogeneous lysosomes present within the cross-section of one cell have been analyzed by the reduced raster method. With one exception (L2) both elements are present in all lysosomes and in the cytoplasm. The mean cerium unit values are significantly different between the "inside" and "outside" points within the reduced rasters applied. The individual lysosomal cerium values did not vary very much (CV = 20-30%) as did the mean cerium value over the whole small population (CV = 13%). The cerium content in the cytoplasm was rather low and consistent. The individual lysosomal iron content, where present, varied considerably (CV = generally around 50-60%). Guided by the absence of iron but presence of cerium, lysosome 2 is considered to be a primary lysosome. Supposedly, when the treatment (flebotomy) at the single cellular level starts to be effective, apparently most, if not all, of the iron storage-vacuoles are tackled by the very recently produced primary lysosomes. However (by treating the figures in the arrays obtained as representing a homogeneous elemental distribution) the heterogeneity of the iron is directly monitored by the high individual or population standard deviation from the respectively calculated mean values (CV = 50-60% and around 90%). And therefore, the overall application requires considerable attention, before the heterogeneity of the elements can be expressed in a logical way.

By the ability to superimpose the various elemental delineations over the other elemental arrays, it becomes possible to differentiate the total grey value of a particle into local elemental contributions (Figs. 15-16). Moreover, by varying the threshold values within a single elemental array the lowest and highest concentrations can be shown and converted into absolute values by analyzing co-embedded Chelex standard beads or any other standard containing the element(s) of interest. But how to handle all these various concentration levels over a total lysosomal population within one cell, or within several liver parenchymal cells within one ultrathin section, still remains to be established in future experiments.

REFERENCES

1. Barbi, NC. (1979). Quantitative methods in biological X-ray microanalysis. Scanning Electron Microsc. 1979;II:659-672.
2. Chandler, JA. (1979). Principles of X-ray microanalysis in biology. Scanning Electron Microsc. 1979;II:595-606.
3. De Bruijn, WC. (1981). Ideal standards for quantitatiave X-ray microanalysis of biological specimens. Scanning Electron Microsc. 1981;II: 357-367.
4. De Bruijn, WC., Zeelen, JPh. (1983). Combined image and X-ray microanalysis of biological material. Beitr. Elektronenmikr. Direktabb. Oberfl. 16, 385-388.
5. De Bruijn, WC. (1984). Standards for quantitative X-ray microanalysis of biological specimens. J. de Phys. Colloq. C2 Suppl. Tome 45, 469-472.
6. De Bruijn, WC., Zeelen, JPh. (1984). Integrated X-ray and morphometric analysis in ultrathin sections. Proc.s 8th European Congress on EM, Budapest, Hungary, p. 1711.(MOTESZ Budapest)
7. De Bruijn, WC. (1985). Integration of X-ray microanalysis and morphometry of biological material. Scanning Electron Microsc. 1985;II: 697-713.
8. McCarthy, JJ., Schamber, FH. (1981). Least--squares fit with digital filter: A status report. In: Energy dispersive X-ray spectrometry (Heinrich, KFJ., Newbury, DE., Myklebust, RL., Fiori, CE., eds). US Dept. Commerce, National Bureau of Standards, Washington, DC., pp. 273-297.
9. Roomans, GM. (1979). Standards for X-ray microanalysis of biological specimens. Scanning Electron Microsc. 1979;II:649-657.
10. Shuman, H., Somlyo, AV., Somlyo, P. (1976). Quantitative electron probe microanalysis of biological thin sections: methods and validity. Ultramicroscopy 1, 317-339.

Discussion with Reviewers

Reviewer 1: The method used for defining the "inside" VS. "outside" boundaries which are overlayed on the background arrays (figures 4 and 5, 9 and 10, 13 and 14) seems somewhat arbitrary. In figures 4 and 5 you use a different threshold value from that used for either the PM or PT arrays; in figures 9 and 10, the boundary seems to be taken directly from the PT array; in figures 13 and 14 the boundary seems to be taken directly from the PM array. This raises several questions: (a) what rationale was employed to define the boundary to be used for the background arrays?; (b) how sensitive are the results to the choice of boundary?; and (c) what criteria would you suggest should be used for an on-line procedure?
Authors: The methods of how to apply the boundaries to the arrays are discussed in our second paper in this volume (text ref. 7). In the past the only other rationale employed to define the boundaries was to compare visually the picture on the colour screen with the original image on the STEM-screen. In the first up-date of the program, the computer was instructed to calculate the mean net-intensity value for the "outside" the particle part of the reduced raster area. In addition the mean value plus twice the standard deviation is given. (See the top-captions of the figures). It was assumed that, prior to the acquisition of the requested structure in the ultrathin section (or inside the cell), the acquisition of a reduced raster analysis of the Epon area (or the cytoplasmic area), to which no threshold had been applied, would give the requested delineation figure (either for the Epon to the cytoplasm, or for the delineation of the cytoplasm from the particle). So far, we have not applied this approach yet, but from the figures presented in the Tables 1 to 3, it can be deduced that this will work. Moreover, several other algorithms are also known to solve this delineation problem. The main reason to introduce several other delineation figures into the arrays, as given in the Tables, and of which only a few are shown in Figs. 2-4 and 7-10, was to learn to what extent the final conclusions were influenced by delineation figure chosen. This influence was only minimally present and can be partially sensed from the results presented in Table 4, where, in addition to the deconvolution method, the influence of the delineation figure is also given (41.8 to 43.4% and 36.5 to 39.8% w/w). It has to be realized that the delineation figures presented are influenced by the instrumental conditions operative during the acquisition of the array. So the conditions operative for the threshold figure 11, applied during the acquisition of the boundary in the erythrocyte array, differ from those under which the Chelex standard was analyzed a few days later. The acquisition of the Chelex Pt-standard and the eosinophilic granule was performed on the same day. Our method of choice, for the time being, would be: first, to acquire the arrays from the Epon and cytoplasm then, to calculate the boundary values, for these two main steps, from the acquired arrays and subsequently perform the reduced raster analyses over the requested particles (and standard) under the same instrumental conditions, with the calculated boundaries introduced into each array. It should be emphasized that the standard beads in the ultrathin section can be used to battle the day to day variations, by matching the figures of the standard with those obtained from the day before, by manipulation of the beam intensity (see Fig. 26 in (7)).

Reviewer 1: In experiment 1 you utilized Lα data for both the SRS and DBL modes but in experiment 2 you utilized Lα data for the DBL mode and Mα data for the SRS mode. Did you perform any experiments where the use of the L and M peaks was compared for the same sample? Wouldn't it also be possible to utilize the M peak for the DBL method? Do you have any opinion as to which peak is preferable for this technique?
Authors: We did not perform the experiment exactly as you suggested, but with some slight alterations. In experiment 1 we demonstrated that both the SRS and the DBL method could be applied centered around the Lα peak of platinum. Both methods resulted in the same final Pt-concentration (Table 1). The application of the DBL method around the Mα-peak of platinum (using a linear relation to acquire the background under the peak) is not advisable for the Mα-region of Pt. We used the Mα-SRS-method in relation to the Lα-DBL method to justify our choice in the past. The constant ratio between the SRS(Mα) and the DBL(Lα) values (Table 7) gives the impression that conversion into absolute values, using the Chelex standards, would produce equal concentration values. This because the values shown in Table 4 are also alike and the ratio between the SRS and DBL values is the same as is indicated in Table 6 and 7. So both methods have their pros and cons and have to be selected accordingly.

Reviewer 1: I am assuming that the standard deviation values quoted in Table 5 (A) are actually the uncertainties in the individual measurements rather than the uncertainty of the mean. Assuming then that the apparent upward trend in mean values with reduced magnification is statistically significant, I am interested in whether the authors have postulated a specific mechanism which could cause this effect. Specifically, I am led to wonder whether this effect would also be manifested as a particle-size dependency. Could the authors please comment?
Authors: The upward trend of the mean values in Table 5 with reduced magnification came as a surprise to us. So far we have indicated a way to alleviate the problem (viz. use the same magnification for the standard and the unknown, which is an acceptable practice) without paying much attention to it. As the homogeneity of the Chelex beads, as demonstrated from the small experiment shown in Table 6, was much more acceptable, especially for the lower magnifications, we prefer to seek the solution to the problem in the optical system of the microscope. The first idea is that the specimen tilt causes the increase; e.g. the points far away from the tilting axis are out of focus (Ø C2 aperture = 150 μm).

D.C. Joy: I never quite discovered the count rates obtained. The authors seem to be using relatively short acquisition times per pixel (one second is mentioned) but no absolute figures are

provided.
Authors: The dwell time per pixelpoint is 1 second. The actual count rate can be deduced from the figures presented in the arrays shown in Figs. 2,7, and 11 for "inside the particle". In practice the actual figures are somewhat higher, as the virtually empty background region Zero is subtracted (on-line). The height of the figure is restricted to 255 c/p/s, which, depending on the local concentration and the applied beam conditions can be (easily) reached and even surpassed. See the net-intensity values for the lysosomes 5 and 6 in Table 8, which are the unit values in c/p/s/nm^2, where the actual figures in c/p/s are 2 x 10^3 higher). In the previous paper (7) the consequences of this 255 limit are discussed.

D.C. Joy: I also wonder whether the habit of quoting figures to two or three significant figures really represents the precision of this data.
Authors: In the Tables 1-8, the mean figures and the standard deviation are acquired from 256 points (16 x 16), present in each reduced raster area. These values are truncated now to one figure behind the decimal point. The coefficient of variance, as given in Table 8 for the cerium distribution within each lysosome, is rather small (13%), whereas generally a figure around 35% is obtained.

D.C. Joy: Some comments about the absolute beam dose and the experience gained with radiation damage would also be very helpful in assessing the usefulness of this technique.
Authors: We are not in a position to measure the actual beam dose in our microscope. The figures given before (7) were values measured at the isolated C2 aperture. These values are not abnormal with respect to the beam doses, given under normal X-ray analytical conditions. In our microscope the specimen area is constantly cooled with liquid nitrogen, which, in combination with the ultra-high vacuum of the ion-getter pump, at least prevents any visual accumulation of matter. Mass-loss is present, though considered to be of normal proportions, especially when the short dwell time per pixelpoint is taken into consideration.

G.M. Roomans: I would suggest that the conversion of the calculated values from c/p/s/nm^2 is omitted. The conversion is not really physically relevant, since the spot size is not identical to the analyzed volume. The conversion does not provide meaningful extra information and makes the Tables more complicated.
Authors: We agree with the reviewer that the conversion of the c/p/s values into c/p/s/nm^2 makes the tables more complicated, and that the same conclusion could have been reached if the c/p/s values of most of the experiments performed had not been converted. However, we disagree that the conversion is not physically relevant. The conversion into unit values is performed by dividing the mean c/p/s values by the calculated area of the beam. Assuming that the ultrathin section is equally thick at the two places to be compared, the result will be independent of the thickness, and accordingly the volume can be replaced by the area. We have to admit that only the results presented in Table 7 deserve the disputed conversion, whereas those in Tables 1-3 can do without. But also the comparison between the point and reduced raster analysis also needed the conversion. As (in the present paper) this conversion however, has been applied at so many places, we suggest that the present form of the (converted) figures should be accepted.